

Glينو reach and mass extraction at the LHC in radiatively-driven natural SUSY

Howard Baer^{1,a}, Vernon Barger^{2,b}, James S. Gainer^{3,c}, Peisi Huang^{4,5,6,d}, Michael Savoy^{1,e}, Dibyashree Sengupta^{1,f}, Xerxes Tata^{3,g}

¹ Department of Physics and Astronomy, University of Oklahoma, Norman, OK 73019, USA

² Department of Physics, University of Wisconsin, Madison, WI 53706, USA

³ Department of Physics and Astronomy, University of Hawaii, Honolulu, HI 96822, USA

⁴ Enrico Fermi Institute, University of Chicago, Chicago, IL 60637, USA

⁵ HEP Division, Argonne National Laboratory, 9700 Cass Ave., Argonne, IL 60439, USA

⁶ Mitchell Institute for Fundamental Physics and Astronomy, Texas A&M University, College Station, TX 77843, USA

Received: 12 April 2017 / Accepted: 14 July 2017 / Published online: 27 July 2017

© The Author(s) 2017. This article is an open access publication

Abstract Radiatively-driven natural SUSY (RNS) models enjoy electroweak naturalness at the 10% level while respecting LHC sparticle and Higgs mass constraints. Glينو and top-squark masses can range up to several TeV (with other squarks even heavier) but a set of light Higgsinos are required with mass not too far above $m_h \sim 125$ GeV. Within the RNS framework, gluinos dominantly decay via $\tilde{g} \rightarrow t\tilde{t}_1^*$, $\tilde{t}_1 \rightarrow t\tilde{t}\tilde{Z}_{1,2}$ or $t\tilde{b}\tilde{W}_1^- + c.c.$, where the decay products of the higgsino-like \tilde{W}_1 and \tilde{Z}_2 are very soft. Glينو pair production is, therefore, signaled by events with up to four hard b -jets and large \cancel{E}_T . We devise a set of cuts to isolate a relatively pure gluino sample at the (high-luminosity) LHC and show that in the RNS model with very heavy squarks, the gluino signal will be accessible for $m_{\tilde{g}} < 2400$ (2800) GeV for an integrated luminosity of 300 (3000) fb^{-1} . We also show that the measurement of the rate of gluino events in the clean sample mentioned above allows for a determination of $m_{\tilde{g}}$ with a statistical precision of 2–5% (depending on the integrated luminosity and the gluino mass) over the range of gluino masses where a 5σ discovery is possible at the LHC.

1 Introduction

Supersymmetric (SUSY) models of particle physics are strongly motivated because they provide a solution to the gauge hierarchy problem (GHP) [1, 2] which arises when the spin zero Higgs sector of the standard model (SM) is coupled to a high mass sector as, for instance, in a grand unified theory (GUT). SUSY models are indirectly supported by data in that: (1) the measured values of the three gauge coupling strengths unify in the minimal supersymmetrized standard model (MSSM) [3–6], (2) the top-quark mass is measured to lie in the range required by SUSY to trigger a radiative breakdown of electroweak symmetry [7–14], for a review, see [15] and (3) the measured value of the Higgs boson mass [16, 17] lies squarely within the range required by the MSSM [18–20]. For a review, see e.g. [21]. However, so far no unambiguous signal for superparticles has emerged from LHC searches [22–24]. In the case of the gluino, \tilde{g} , (the spin-1/2 superpartner of the gluon), recent search results in the context of simplified models place mass limits as high as $m_{\tilde{g}} \gtrsim 1500$ –1900 GeV [25–27] for a massless lightest SUSY particle (LSP), depending on the assumed decay of the gluino. This may be contrasted with early expectations from naturalness, such as the Barbieri–Giudice (BG) $\Delta_{\text{BG}} < 30$ bounds [28], this measure was introduced in [29], which required $m_{\tilde{g}} \lesssim 350$ GeV.¹

^a e-mail: baer@ou.edu

^b e-mail: barger@pheno.wisc.edu

^c e-mail: jgainer@hawaii.edu

^d e-mail: huang@physics.tamu.edu

^e e-mail: savoy@ou.edu

^f e-mail: Dibyashree.Sengupta-1@ou.edu

^g e-mail: tata@phys.hawaii.edu

¹ Barbieri and Giudice obtained upper bounds on superpartner masses requiring $\Delta_{\text{BG}} < 10$. We have translated their result and cited the bound $m_{\tilde{g}} \leq 350$ GeV, using $\Delta_{\text{BG}} < 30$ to enable direct comparison with upper limits obtained using $\Delta_{\text{EW}} < 30$. The onset of fine-tuning for $\Delta_{\text{EW}} \gtrsim 30$ is visually displayed in Fig. 1 of Ref. [30].

Likewise, LHC simplified model analyses typically require $m_{\tilde{t}_1} \gtrsim 700 - 850$ GeV [26,27,31,32] to be contrasted with Dimopoulos–Giudice (DG) $\Delta_{BG} < 30$ fine-tuning bounds [33] that require $m_{\tilde{t}_1} \lesssim 500$ GeV or with Higgs mass large log bounds [34,35] which require *three* third generation squarks of mass $\lesssim 500$ GeV. Conflicts such as these have led many to question whether weak scale SUSY is indeed nature’s chosen solution to the GHP, or whether nature follows some entirely different direction [36]; see also [37], [38,39].

A more conservative approach to naturalness has been adopted in Refs. [40,41]. Here, one requires that there are no large cancellations among the various terms on the right-hand side of the well-known expression that yields the measured value of m_Z in terms of the weak scale SUSY Lagrangian parameters via the scalar potential minimization condition, implemented at the optimized scale choice $Q = \sqrt{m_{\tilde{t}_1} m_{\tilde{t}_2}}$:

$$\frac{m_Z^2}{2} = \frac{m_{H_d}^2 + \Sigma_d^d - (m_{H_u}^2 + \Sigma_u^u) \tan^2 \beta}{\tan^2 \beta - 1} - \mu^2 \simeq -m_{H_u}^2 - \Sigma_u^u - \mu^2. \tag{1}$$

The Σ_u^u and Σ_d^d terms in Eq. (1) arise from 1-loop corrections to the scalar potential (expressions can be found in the appendix of Ref. [41]), $m_{H_u}^2$ and $m_{H_d}^2$ are the soft SUSY breaking Higgs mass parameters, $\tan \beta \equiv \langle H_u \rangle / \langle H_d \rangle$ is the ratio of the Higgs field VEVs and μ is the superpotential (SUSY conserving) Higgs/higgsino mass parameter. SUSY models requiring large cancellations between the various terms on the right-hand-side of Eq. (1) to reproduce the measured value of m_Z^2 are regarded as unnatural, or fine-tuned. Thus, the *electroweak* naturalness measure, Δ_{EW} , is given by the maximum value of the ratio of each term on the right-hand-side of Eq. (1) and $m_Z^2/2$.

This conservative approach to naturalness allows for the possibility that high-scale parameters that have been taken to be independent will, in fact, turn out to be correlated once SUSY breaking is understood. Ignoring these correlations will lead to an overestimate of the UV sensitivity of a theory, making it appear to be fine-tuned. In Ref. [42–44] it is argued that if all correlations among parameters are correctly implemented the conventional Barbieri–Giudice measure reduces to Δ_{EW} and that a high-scale theory that predicts these parameter correlations would be natural. We urge using the more conservative electroweak measure for discussions of naturalness since disregarding the possibility of parameter correlations may lead to prematurely discarding what may be a perfectly viable effective theory.

For SUSY models with electroweak naturalness, we have:

- $|\mu| \sim 100\text{--}300$ GeV (the closer to m_Z the more natural) leading to the requirement of four light higgsinos $\tilde{Z}_{1,2}$ and \tilde{W}_1^\pm of similar mass values $\sim |\mu|$,
- $m_{H_u}^2$ must be driven radiatively to small negative values $\sim -(100\text{--}300)^2$ GeV² at the weak scale (for this reason, these models are said to exhibit radiatively-driven naturalness, and have been dubbed radiatively-driven natural SUSY (RNS) [40,41]).
- the radiative corrections $|\Sigma_u^u(i)| \lesssim (100\text{--}300)^2$ GeV². The largest of these typically arise from the top squarks and require for $\Delta_{EW} < 30$ that $m_{\tilde{t}_1} \lesssim 3$ TeV, a factor 10 higher than the aforementioned BG/DG bounds. Gluinos contribute to Σ_u^u at two-loop order [35] and in models with gaugino mass unification, then $m_{\tilde{g}} \lesssim 4$ TeV [30,41,46].

We see that SUSY models with electroweak naturalness can easily respect LHC sparticle mass bounds and are in accord with the measured value of m_h , which requires large mixing among top squarks [47].

What of LHC signatures in RNS models? Old favorites like searches for gluino pairs ($pp \rightarrow \tilde{g}\tilde{g}X$ where X represents assorted hadronic debris) are still viable where now $\tilde{g} \rightarrow \tilde{t}_1 t$ if kinematically allowed or $\tilde{g} \rightarrow t\tilde{t}\tilde{Z}_i$ or $t\tilde{b}\tilde{W}_j$ when $m_{\tilde{g}} < m_{\tilde{t}_1} + m_t$ [48,49]. In the case of RNS, the $m_{\tilde{g}} - m_{\tilde{Z}_1}$ mass gap is expected to be *larger* than in models such as CMSSM/mSUGRA where the \tilde{Z}_1 is typically bino-like. In addition, for RNS, the \tilde{Z}_2 produced in gluino cascade decays leads to the presence of opposite-sign/same flavor dilepton pairs with $m(\ell^+\ell^-) < m_{\tilde{Z}_2} - m_{\tilde{Z}_1} \sim 10\text{--}20$ GeV [50,51]. However, new signatures also arise for RNS. Wino pair production $pp \rightarrow \tilde{W}_2\tilde{Z}_4$ can occur at large rates leading to the low background same-sign diboson signature from $\tilde{W}_2 \rightarrow W^+\tilde{Z}_{1,2}$ and $\tilde{Z}_4 \rightarrow W^+\tilde{W}_1^-$ decays [50,52]. This very clean signature leads to the greatest reach for SUSY in the $m_{1/2}$ direction for an integrated luminosity $L \gtrsim 100\text{--}200$ fb⁻¹. Also, direct higgsino pair production $pp \rightarrow \tilde{Z}_1\tilde{Z}_2 j$ followed by $\tilde{Z}_2 \rightarrow \ell^+\ell^-\tilde{Z}_1$ decay offers substantial reach in the μ direction of parameter space [53–55]. Combined, the latter two signatures offer high-luminosity (HL) LHC a complete coverage of RNS SUSY with unified gaugino masses for $\Delta_{EW} < 30$ and $L \sim 3000$ fb⁻¹ [56]. In addition to LHC searches, an International Linear e^+e^- Collider (ILC) with $\sqrt{s} \gtrsim 500\text{--}600$ GeV $> 2m(\text{higgsino})$ would be a *higgsino factory* and completely cover the $\Delta_{EW} \leq 30$ RNS parameter space and allow precision measurements that would serve to elucidate the natural origin of W , Z and Higgs boson masses [57,58].

Although the discovery of the gluino at the LHC is not guaranteed over the viable RNS parameter space, we re-examine gluino pair production signatures expected within the RNS framework. Our purpose is first, to delineate the

gluino reach of LHC14 and its high-luminosity upgrade, and second, to study the extent to which the gluino mass may be extracted at the LHC. Although not required by naturalness, one usually takes first and second generation matter scalar mass parameters, assumed unified to a value m_0 at scale $Q = m_{\text{GUT}}$, to be in the multi-TeV range. This alleviates the SUSY flavor problem with little impact on naturalness as long as these scalars satisfy well-motivated intra-generational degeneracy patterns [59]. For integrated luminosities in excess of 100 fb^{-1} , which should be accumulated within the next few years, we show that judicious cuts can be found so that the gluino pair production signal emerges with very little SM background in the data sample, allowing for a gluino reach well beyond the expectation within the mSUGRA/CMSSM framework. Moreover, assuming decoupled first and second generation squarks, the measured event rate from the gluino signal depends *only* on the value of $m_{\tilde{g}}$. The rate for gluino events after cuts that eliminate most of the SM background can, therefore, be used to extract the gluino mass, assuming that gluino events as well as the experimental detector can be reliably modeled. This “counting rate” method of extracting $m_{\tilde{g}}$ [60] has several advantages over the kinematic methods which have been advocated [61–65]. It remains viable even if a variety of complicated cascade decay topologies are expected to be present. In addition, it is unaffected by ambiguities over which jets or leptons are to be associated with which of the two gluinos that are produced. We explore the counting rate extraction of $m_{\tilde{g}}$ in RNS SUSY and find it typically leads to extraction of $m_{\tilde{g}}$ with a statistical precision of 2–5%, depending on the value of $m_{\tilde{g}}$ and the assumed integrated luminosity, ranging between 300–3000 fb^{-1} .

The rest of this paper is organized as follows. In Sect. 2 we present the RNS model line that we adopt for our analysis and briefly describe the event topologies expected from gluino pair production within the RNS framework using a benchmark point with $m_{\tilde{g}} = 2 \text{ TeV}$ for illustration. In Sect. 3, we discuss details of our simulation of the SUSY signal as well as the relevant SM backgrounds. In Sect. 4 we describe the analysis cuts to select out gluino events from SM backgrounds and show that it is possible to reduce the background level to no more 3% for our benchmark case. In Sect. 5.1 we show our projections for the mass reach for gluinos in the RNS framework, while in Sect. 5.2 we show the precision with which $m_{\tilde{g}}$ may be extracted at the LHC. Finally, we summarize our results in Sect. 6.

2 An RNS model line

To facilitate the examination of gluino signals in models with natural SUSY spectra, we adopt the RNS model line first introduced in Ref. [50] (except that we now take $\tan \beta =$

Table 1 NUHM2 input parameters and masses in GeV units for a *radiatively-driven natural SUSY* benchmark points introduced in the text. We take $m_t = 173.2 \text{ GeV}$

| Parameter | Value |
|--|----------------------|
| m_0 | 5000 |
| $m_{1/2}$ | 800 |
| A_0 | −8000 |
| $\tan \beta$ | 10 |
| μ | 150 |
| m_A | 1000 |
| $m_{\tilde{g}}$ | 2007.8 |
| $m_{\tilde{u}_L}$ | 5169.3 |
| $m_{\tilde{u}_R}$ | 5322.7 |
| $m_{\tilde{c}_R}$ | 4808.0 |
| $m_{\tilde{t}_1}$ | 1479.3 |
| $m_{\tilde{t}_2}$ | 3650.1 |
| $m_{\tilde{b}_1}$ | 3678.3 |
| $m_{\tilde{b}_2}$ | 5049.3 |
| $m_{\tilde{\tau}_1}$ | 4734.4 |
| $m_{\tilde{\tau}_2}$ | 5079.7 |
| $m_{\tilde{\nu}_\tau}$ | 5087.0 |
| $m_{\tilde{W}_2}$ | 691.3 |
| $m_{\tilde{W}_1}$ | 155.3 |
| $m_{\tilde{Z}_4}$ | 702.2 |
| $m_{\tilde{Z}_3}$ | 362.8 |
| $m_{\tilde{Z}_2}$ | 158.2 |
| $m_{\tilde{Z}_1}$ | 142.4 |
| m_h | 124.4 |
| $\Omega_{\tilde{Z}_1}^{\text{std}} h^2$ | 0.008 |
| $BF(b \rightarrow s\gamma) \times 10^4$ | 3.3 |
| $BF(B_s \rightarrow \mu^+\mu^-) \times 10^9$ | 3.8 |
| $\sigma^{SI}(\tilde{Z}_1 p)$ (pb) | 4.3×10^{-9} |
| Δ_{EW} | 10.3 |

10). Specifically, we work within the framework of the two extra parameter non-universal Higgs model (NUHM2) [66–70] with parameter inputs,

$$m_0, m_{1/2}, A_0, \tan \beta, \mu, m_A \quad (\text{NUHM2}). \tag{2}$$

We use Isajet/Isasugra 7.85 spectrum generator [71] to obtain sparticle masses. For our model line, we adopt parameter choices $m_0 = 5000 \text{ GeV}$, $A_0 = -8000 \text{ GeV}$, $\tan \beta = 10$, $\mu = 150 \text{ GeV}$ and $m_A = 1000 \text{ GeV}$, while $m_{1/2}$ varies across the range 600–1200 GeV corresponding to a gluino mass range of $m_{\tilde{g}} \sim 1600\text{--}2800 \text{ GeV}$, i.e., starting just below present LHC bounds on $m_{\tilde{g}}$ and extending just beyond the projected reach for HL–LHC. The spectrum, together with some low energy observables, is illustrated for a benchmark point with $m_{\tilde{g}} \simeq 2000 \text{ GeV}$ in Table 1. Along this model line,

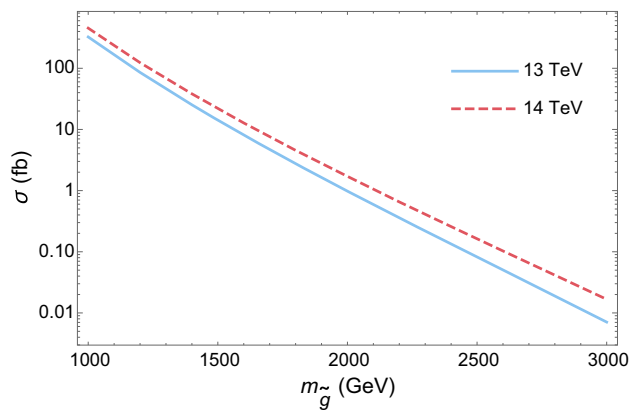


Fig. 1 Total NLO+NLL cross section for $pp \rightarrow \tilde{g}\tilde{g}X$ at LHC with $\sqrt{s} = 13$ and 14 TeV, versus $m_{\tilde{g}}$ for $m_{\tilde{q}} \simeq 5$ TeV

the computed value of the light Higgs mass is quite stable and varies over $m_h : 124.1\text{--}124.7$ GeV. (We expect a couple GeV theory error in our RG-improved one loop effective potential calculation of m_h which includes leading two-loop effects.) The value of Δ_{EW} varies between 8.3–24 along the model line so the model is very natural with electroweak fine-tuning at the 12–4% level.

The cross section for $pp \rightarrow \tilde{g}\tilde{g}X$, calculated using Prospino [72] with NLL-FAST [73], is shown in Fig. 1 vs. $m_{\tilde{g}}$ for $m_{\tilde{q}} \simeq 5$ TeV and for $\sqrt{s} = 13$ and 14 TeV. For $m_{\tilde{g}} \sim 2$ TeV and $\sqrt{s} = 14$ TeV—the benchmark case that we adopt for devising our analysis cuts— $\sigma(\tilde{g}\tilde{g}) \sim 1.7$ fb; the cross section drops to about $\sigma \sim 0.02$ fb for $m_{\tilde{g}} \sim 3$ TeV.

Once the gluinos are produced, all across the model line they decay dominantly via the 2-body mode $\tilde{g} \rightarrow \tilde{t}_1\bar{t}$ or \tilde{t}_1^*t , because all other squarks are heavier than the gluino. For the benchmark point in Table 1, the daughter top squarks rapidly decay via $\tilde{t}_1 \rightarrow b\tilde{W}_1$ at $\sim 50\%$, $t\tilde{Z}_1$ at $\sim 20\%$, $t\tilde{Z}_2$ at $\sim 24\%$ and $t\tilde{Z}_3$ at $\sim 6\%$. Stop decays into $b\tilde{W}_2$ and $t\tilde{Z}_4$ are suppressed since in our model with stop soft masses unified at m_0 at the GUT scale, then the \tilde{t}_1 is mainly a right-stop eigenstate with suppressed decays to winos. The stop branching fractions vary hardly at all as $m_{1/2}$ varies along the model line. The higgsino-like \tilde{Z}_1 state is expected to comprise a portion of the dark matter in the universe (the remaining portion might consist of, e.g., axions [74–76]) while the higgsino-like \tilde{Z}_2 and \tilde{W}_1 decay via 3-body modes to rather soft visible debris because the mass gaps $m_{\tilde{Z}_2} - m_{\tilde{Z}_1}$ and $m_{\tilde{W}_1} - m_{\tilde{Z}_1}$ are typically only 10–20 GeV and hence essentially invisible for the purposes of this paper.

Putting together production and decay processes, gluino pair production final states consist of $t\bar{t}t\bar{t} + \cancel{E}_T$, $t\bar{t}b\bar{b} + \cancel{E}_T$ and $t\bar{t}b\bar{b} + E_T$ parton configurations, where \cancel{E}_T refers to missing transverse energy. (Transverse energy itself is represented by E_T .) In the case where \tilde{Z}_2 is produced via the gluino cascade decays, then the boosted decay products from $\tilde{Z}_2 \rightarrow \ell^+\ell^-\tilde{Z}_1$ decay may display an invariant mass edge

$m(\ell^+\ell^-) < m_{\tilde{Z}_2} - m_{\tilde{Z}_1} \sim 10\text{--}20$ GeV. The existence of such an edge in gluino cascade decay events containing an OS/SF dilepton pair would herald the presence of light higgsinos [50, 51] though the cross sections for these events are very small. In this paper, our focus will be on the observation of the signal and prospects for gluino mass reconstruction using the inclusive sample with $t\bar{t}t\bar{t} + \cancel{E}_T$, $t\bar{t}b\bar{b} + \cancel{E}_T$ and $t\bar{t}b\bar{b} + E_T$ final states, with no attention to how the final state higgsinos (which are produced in the bulk of the cascade decays) decay.

3 Event generation

We employ two procedures for event generation, one using ISAJET 7.85 [71], which we refer to as our “Isajet” simulation and one using MADGRAPH 2.3.3 [77, 78] interfaced to PYTHIA 6.4.14 [79] with detector simulation by DELPHES 3.3.0 [80], which we refer to as our “MadGraph” simulation.

3.1 Isajet simulation

Our Isajet simulation includes detector simulation by the Isajet toy detector, with calorimeter cell size $\Delta\eta \times \Delta\phi = 0.05 \times 0.05$ and $-5 < \eta < 5$. The HCAL energy resolution is taken to be $80\%/\sqrt{E} \oplus 3\%$ for $|\eta| < 2.6$ and $100\%/\sqrt{E} \oplus 5\%$ for $|\eta| > 2.6$, where “ \oplus ” denotes combination in quadrature. The ECAL energy resolution is assumed to be $3\%/\sqrt{E} \oplus 0.5\%$. We use a UA1-like jet finding algorithm with jet cone size $R = 0.4$ and require that $E_T(\text{jet}) > 50$ GeV and $|\eta(\text{jet})| < 3.0$. Leptons are considered isolated if they have $p_T(e \text{ or } \mu) > 20$ GeV and $|\eta| < 2.5$ with visible activity within a cone of $\Delta R < 0.2$ of $\sum E_T^{\text{cells}} < 5$ GeV. The strict isolation criterion helps reduce multi-lepton backgrounds from heavy quark ($c\bar{c}$ and $b\bar{b}$) production.

We identify a hadronic cluster with $E_T > 50$ GeV and $|\eta(\text{jet})| < 1.5$ as a b -jet if it contains a B hadron with $p_T(B) > 15$ GeV and $|\eta(B)| < 3$ within a cone of $\Delta R < 0.5$ around the jet axis. We adopt a b -jet tagging efficiency of 60% and assume that light quark and gluon jets can be mistagged as b -jets with a probability of $1/150$ for $E_T < 100$ GeV, $1/50$ for $E_T > 250$ GeV and a linear interpolation for $100 \text{ GeV} < E_T < 250 \text{ GeV}$.² We refer to these values as our “Isajet” parameterization of b -tagging efficiencies.

3.2 MadGraph simulation

In our MadGraph simulation, the events are showered and hadronized using the default MadGraph/PYTHIA interface

² These values are based on ATLAS studies of b -tagging efficiencies and rejection factors in $t\bar{t}H$ and WH production processes [81, 82].

with default parameters. Detector simulation is performed by Delphes using the default Delphes 3.3.0 “CMS” parameter card with several changes, which we enumerate here.

1. We set the HCAL and ECAL resolution formulas to be those that we have used in our Isajet simulation.
2. We turn off the jet energy scale correction.
3. We use an anti- k_T jet algorithm [83] with $R = 0.4$ rather than the default $R = 0.5$ for jet finding in Delphes (which is implemented via FASTJET [84]). As in our Isajet simulation, we only consider jets with $E_T(\text{jet}) > 50 \text{ GeV}$ and $|\eta(\text{jet})| < 3.0$ in our analysis. The choice of $R = 0.4$ in the jet algorithm is made both to make our MadGraph simulation conform to our Isajet simulation and to allow comparison with CMS b -tagging efficiencies [85]; see Table 3 below.
4. We write our own jet flavor association module based on the “ghost hadron” procedure [86], which allows decayed hadrons to be unambiguously assigned to jets. With this functionality we identify a jet with $|\eta| < 1.5$ as a b -jet if it contains a B hadron (in which the b quark decays at the next step of the decay) with $|\eta| < 3.0$ and $p_T > 15 \text{ GeV}$. These values are in accordance with our Isajet simulation.
5. We turn off tau tagging, as we do not use the tagging of hadronic taus in our analyses. Sometimes Delphes will wrongly tag a true b -jet as a tau, if the B hadron in the jet decays to a tau. As we are trying to perform a cross section measurement in a regime where the overall signal cross section is small, we did not want to “lose” these b -jets.

3.3 Processes simulated

Our Isajet simulation was used to generate the signal from gluino pair production at our benchmark point, as well as for other parameter points along our model line. We also used our Isajet simulation to simulate backgrounds from $t\bar{t}$, W + jets, Z + jets, WW , WZ , and ZZ production. The W + jets and Z + jets backgrounds use exact matrix elements for one parton emission, but rely on the parton shower for subsequent emissions. In addition, we have generated background events with our Isajet simulation procedure for QCD jet production (jet-types including g , u , d , s , c , and b quarks) over five p_T ranges, as shown in Table II of Ref. [60]. Additional jets are generated via parton showering from the initial and final hard scattering subprocesses.

Our MadGraph simulation was used to generate the signal from gluino pair production at our benchmark point, as well as for other parameter points along our model line. It was also used to generate backgrounds from $t\bar{t}$, $t\bar{t}b\bar{b}$, $b\bar{b}Z$, and $t\bar{t}t\bar{t}$ production as well as from single-top production. To avoid the double counting that would ensue from simulating $t\bar{t}$ as well as $t\bar{t}b\bar{b}$, we veto events with more than two truth b -jets in our $t\bar{t}$ sample.

In simulating $t\bar{t}$, $t\bar{t}b\bar{b}$, single top, and $b\bar{b}Z$ with MadGraph, we generate events in various bins of generator-level \cancel{E}_T . The use of weighted events from this procedure gives us sensitivity to the high tail of the \cancel{E}_T distribution for these background processes. This sensitivity is essential for determining the rates that remain from background processes after the very hard \cancel{E}_T cuts, described in the next section, that we use to isolate the signal.

In our MadGraph simulation, we normalize the overall cross section for our signal to NLL values obtained from NLL-FAST [73]. For $t\bar{t}$ we used an overall cross section of 953.6 pb, following Ref. [87]. As MadGraph chooses the scale dynamically event-by-event, we follow Ref. [88] and use a K-factor of 1.3 for our $t\bar{t}b\bar{b}$ backgrounds; the authors of this work find larger K-factors when a dynamic scale choice is not employed [89]. For the evaluation of the background from $b\bar{b}Z$ production we use a K-factor of 1.5, following Ref. [90], while for the $t\bar{t}t\bar{t}$ backgrounds we use a K-factor of 1.27, following Ref. [91]. For our single-top cross sections we use the ATLAS-CMS recommended predictions [92] which are based on the Hathor v2.1 program [93, 94]. Following this reference we take the total NLO cross section for single-top production processes ($qb \rightarrow q't$ mediated by the t -channel W -exchange for which the NLO cross section is 248.1 pb and $gb \rightarrow Wt$ production for which the NLO cross section is 84.4 pb, together with the electroweak s -channel process, $ud \rightarrow tb$, for which the NLO cross section is 11.4 pb) to be 343.9 pb.

We found very similar results when using signal events from our Isajet simulation procedure as when using signal events from our MadGraph simulation procedure. We found significantly more $t\bar{t}$ events with high values of missing \cancel{E}_T from our MadGraph simulation procedure than we did from our Isajet procedure, presumably due to differences in showering algorithms. To be conservative, we use the larger $t\bar{t}$ backgrounds generated from MadGraph in our analyses. The hard \cancel{E}_T cuts described below together with the requirement of at least two tagged b -jets, very efficiently remove the backgrounds from W , Z + jets and from VV production simulated with Isajet. In the interest of presenting a clear and concise description of our analysis, we will not include these backgrounds in the figures and tables in the remainder of this work. For consistency with the most relevant SM backgrounds from $t\bar{t}$, $Zb\bar{b}$, $t\bar{t}b\bar{b}$, $t\bar{t}t\bar{t}$ and single-top production, we likewise utilize our signal samples generated using the MadGraph simulation procedure. In effect, the entire analysis presented here (for both the signal and the dominant backgrounds) is based on our MadGraph simulation procedure. Our Isajet simulation procedure is only used for backgrounds from W , Z + jet production and from VV production which, we will see, are negligible after the b -jet multiplicity and hard \cancel{E}_T and analysis cuts discussed in the following section.

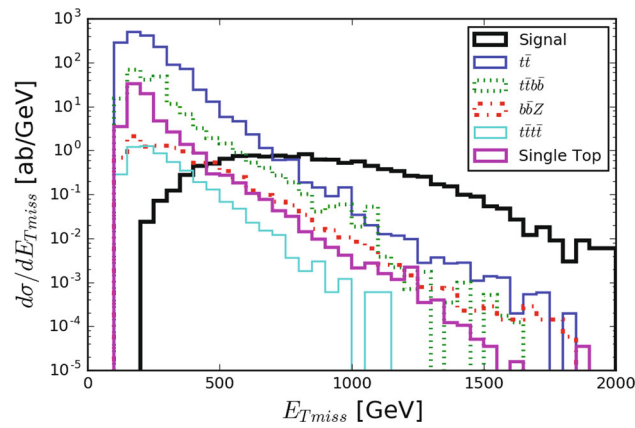


Fig. 2 Distribution of E_T after C1 cuts (3) with the requirement of two b -tagged jets for the gluino pair production signal, as well as the most relevant backgrounds ($t\bar{t}$, $t\bar{t}b\bar{b}$, $b\bar{b}Z$, $t\bar{t}t\bar{t}$ and *single top*)

4 Gluino event selection

To separate the gluino events from SM backgrounds, we begin by applying a set of pre-cuts to our event samples, which we call **C1** (for “cut set 1”). These are very similar to a set of cuts found in the literature [60,95,96]. However, since our focus is on the signal from very heavy gluinos ($m_{\tilde{g}} \geq 1.6 \text{ TeV}$), we have raised the cut on jet p_T to 100 GeV from 50 GeV and included a cut on the transverse mass of the lepton and \cancel{E}_T in events with only one isolated lepton (to reduce backgrounds from events with W bosons).

C1 cuts:

$$\begin{aligned} \cancel{E}_T &> \max(100 \text{ GeV}, 0.2M_{\text{eff}}), \\ n(\text{jets}) &\geq 4, \\ E_T(j_1, j_2, j_3, j_4) &> 100 \text{ GeV}, \\ S_T &> 0.2, \\ m_T(\ell, \cancel{E}_T) &> 150 \text{ GeV, if } n_{lep} = 1. \end{aligned} \tag{3}$$

Here, M_{eff} is defined as in Hinchliffe et al. [95,96] as $M_{\text{eff}} = / E_T + E_T(j_1) + E_T(j_2) + E_T(j_3) + E_T(j_4)$, where $j_1 - j_4$ refer to the four highest E_T jets ordered from highest to lowest E_T , \cancel{E}_T is missing transverse energy, S_T is transverse sphericity,³ and m_T is the transverse mass of the lepton and the \cancel{E}_T .

Since the signal naturally contains a high multiplicity of hard b -partons from the decay of the gluinos because third generation squarks tend to be lighter than other squarks, in addition to the basic **C1** cuts, we also require the presence of two tagged b -jets,

b-jet multiplicity cut:

$$n_b \geq 2, \tag{4}$$

³ Sphericity is defined, e.g., in *Collider Physics*, V. Barger and R. J. N. Phillips (Addison Wesley, 1987). Here, we restrict its construction to using only transverse quantities, as is appropriate for a hadron collider.

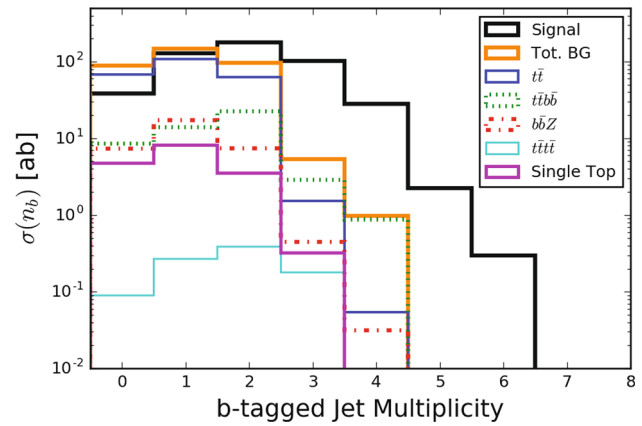


Fig. 3 The number of b -tagged jets, using the Isajet parameterization of the b -tagging efficiency, after C1 cuts (3) and the requirement that $\cancel{E}_T > 750 \text{ GeV}$

using the “Isajet” parameterization of b -tagging efficiencies and light jet mistagging.

Even after these cuts, we must still contend with sizable backgrounds, as can be seen from Fig. 2 where we show the \cancel{E}_T distribution from the $t\bar{t}$, $t\bar{t}b\bar{b}$, $b\bar{b}Z$, $t\bar{t}t\bar{t}$ and *single top* backgrounds, as well as from the gluino pair production for the benchmark point in Table 1. We see that the backgrounds fall more quickly with \cancel{E}_T than the signal leading us to impose a \cancel{E}_T cut,

\cancel{E}_T cut:

$$\cancel{E}_T > 750 \text{ GeV}. \tag{5}$$

After this cut, we are left with comparable backgrounds from $t\bar{t}$ and $t\bar{t}b\bar{b}$ production with a somewhat smaller contribution from $b\bar{b}Z$ production. The $t\bar{t}t\bar{t}$ and *single-top* background rates are much smaller.

Once we have made the \cancel{E}_T cut (5), we examine the distribution of the multiplicity of b -tagged jets, with the goal of further improving the signal-to-background ratio. This distribution is shown in Fig. 3. This figure suggests two roads to selection criteria that will leave a robust signal and negligible backgrounds. Obviously, we can require three b -tags, which decimates the backgrounds (especially $t\bar{t}$) at the cost of some signal. Our goal is to devise a strategy that will allow mass measurements even with integrated luminosities of $100\text{--}200 \text{ fb}^{-1}$, which will be available by the end of the 2018 LHC shutdown for which significant loss of event rate rapidly becomes a problem. With this in mind, we also examine the possibility that we can only require two b -tags. While this saves some signal, we clearly need to impose additional cuts to obtain a clean signal sample. We pursue both of these approaches: the larger cross section from the “2b” analysis will certainly be useful in early LHC running, but the greater reduction of backgrounds provided by the “3b” anal-

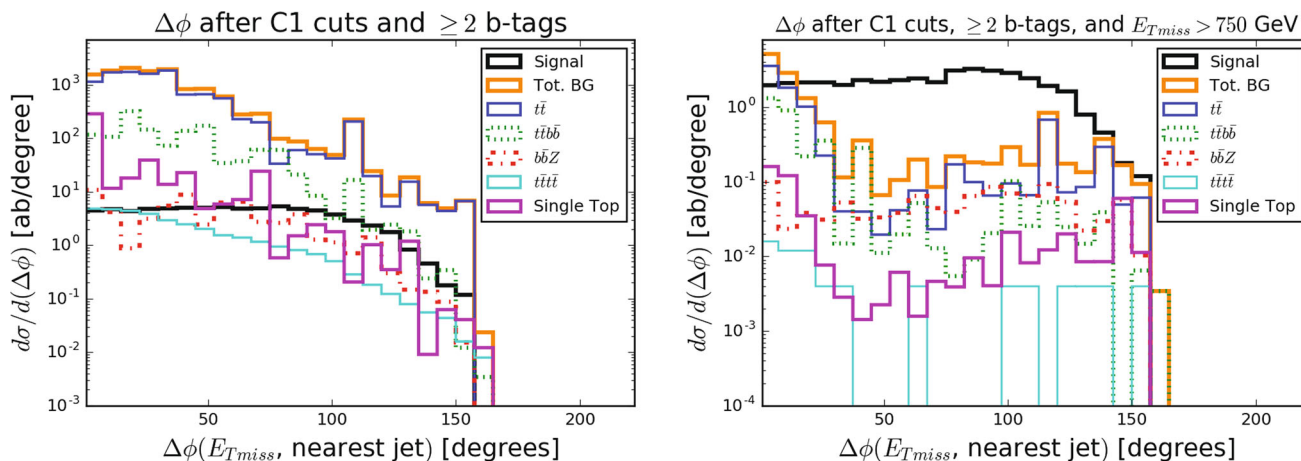


Fig. 4 The distribution of $\Delta\phi(E_T, \text{nearest jet})$. Explicitly this quantity is the minimum angle between the E_T vector and the transverse momentum of one of the leading four jets. This quantity is shown (left)

after C1 cuts (3) with the requirement of two b -tagged jets and (right) after these cuts, and a cut of $E_T > 750 \text{ GeV}$

ysis would be expected to yield cleaner data samples at the high-luminosity LHC.

To further clean up the $n_b \geq 2$ signal sample, we first note that the bulk of the background comes from $t\bar{t}$ production. It is reasonable to expect that $t\bar{t}$ production leads to $E_T > 750 \text{ GeV}$ only if a semi-leptonically decaying top is produced with a very high transverse momentum, with the daughter neutrino “thrown forward” in the top rest frame, while the other top decays hadronically (so the E_T is not canceled). In this case, the b -jet from the decay of the semi-leptonically decaying top would tend to be collimated with the neutrino; i.e., to the direction of E_T . We do not expect such a correlation in the signal since the heavy gluinos need not be particularly boosted to yield $E_T > 750 \text{ GeV}$. This motivated us to examine the distribution of the minimum value of $\Delta\phi$, the angle between the transverse momenta of a jet and the E_T vector, for each of the four leading jets. We show this distribution in Fig. 4, after the C1 and the two tagged b -jet cuts, both with (right frame) and without (left frame) the $E_T > 750 \text{ GeV}$ cut. Without this hard E_T cut, we see that the distribution of $\Delta\phi$ is very slowly falling for the $t\bar{t}$ background, and roughly flat for the signal as for the other backgrounds, until all the distributions cut-off at about 150° . The expected peaking of the $t\bar{t}$ background at low values of $\Delta\phi$ is, however, clearly visible in the right frame, while the signal is quite flat. The next largest backgrounds from $t\bar{t}b\bar{b}$ and single top also show a similar peaking (for the same reason) at low $\Delta\phi$ values. We are thus led to impose the cut, $\Delta\phi$ cut:

$$\Delta\phi(E_T, \text{nearest of four leading jets}) > 30^\circ, \quad (6)$$

which greatly diminishes the dominant backgrounds in the two tagged b -jet channel with only a very modest loss of

signal. Indeed, because the signal-to-background ratio is so vastly improved with only a slight reduction of the signal, we have retained this cut in both our 2b and 3b analyses.

Having made this cut, we return to the E_T distribution, to see whether further optimization might be possible. Toward this end, we show the distribution after the C1 cuts (3), the $E_T > 750 \text{ GeV}$ cut (5), and the $\Delta\phi > 30^\circ$ cut (6) in Fig. 5, requiring at least two b -tagged jets (left panel) or three b -tagged jets (right panel). We see that an additional cut on E_T will be helpful in the 2b analysis, but not as helpful in the 3b analysis. Therefore, our final cut choices are:

2b analysis:

$$\begin{aligned} &\text{C1 cuts,} \\ &n_b \geq 2, \\ &\Delta\phi(E_T, \text{nearest of four leading jets}) > 30^\circ, \\ &E_T > 900 \text{ GeV,} \end{aligned} \quad (7)$$

and

3b analysis:

$$\begin{aligned} &\text{C1 cuts,} \\ &n_b \geq 3, \\ &\Delta\phi(E_T, \text{nearest of four leading jets}) > 30^\circ, \\ &E_T > 750 \text{ GeV,} \end{aligned} \quad (8)$$

The cross section including acceptance after each of the cuts, for the signal benchmark point, as well as for the sum of the $t\bar{t}$, $t\bar{t}b\bar{b}$, $b\bar{b}Z$, $t\bar{t}t\bar{t}$ and single-top backgrounds, is given in Table 2, for both the 2b and the 3b analyses. We expect that it will also be possible to determine these backgrounds directly from the data from the HL-LHC.

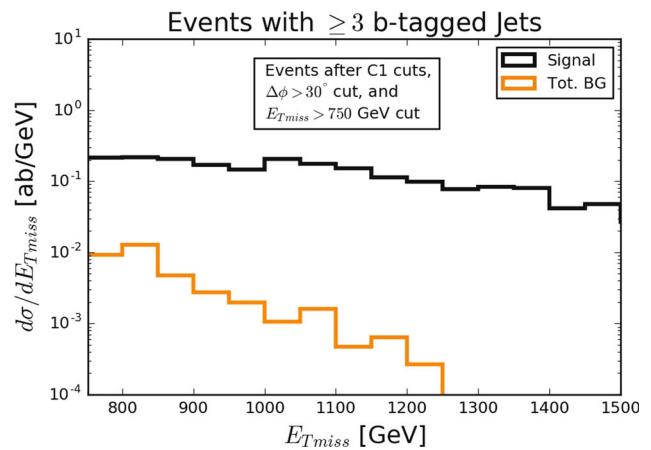
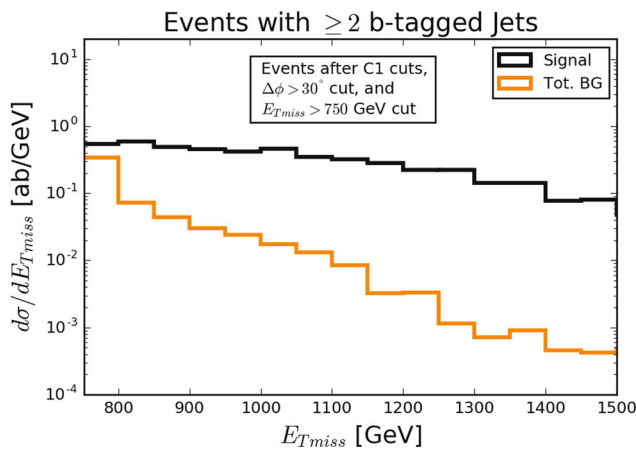


Fig. 5 The distribution of E_T after C1 cuts (3), the $E_T > 750$ cut (5), and the $\Delta\phi > 30^\circ$ cut (6) with the additional requirement of (left) at least two b -tagged jets (right) at least three b -tagged jets. The back-

ground distribution represents the sum of the contributions from the $t\bar{t}$, $t\bar{t}b\bar{b}$, $b\bar{b}Z$, $t\bar{t}t\bar{t}$ and *single-top* backgrounds

Table 2 Cross section times acceptance in attobarns (1000 ab= 1 fb) after various cuts are applied. The “ b -tagging” cut refers to the requirement of ≥ 2 b -tagged jets in the 2b analysis and ≥ 3 b -tagged jets in the 3b analysis. For the 2b analysis, the “final E_T cut” refers to the additional requirement that $E_T > 900$ GeV; there is no additional cut in the 3b analysis

| Cut | 2b Sig. | 2b BG | 3b Sig. | 3b BG |
|-------------------------|---------|--------------------|---------|--------------------|
| C1 | 872 | 5.14×10^5 | 872 | 5.14×10^5 |
| $E_T > 750$ GeV | 479 | 340 | 479 | 340 |
| b -tagging | 311 | 103 | 133 | 6.31 |
| $\Delta\phi > 30^\circ$ | 249 | 28.1 | 105 | 1.78 |
| Final E_T cut | 167 | 5.31 | 105 | 1.78 |

4.1 Gluino event characteristics

Now that we have finalized our analysis cuts, we display the characteristic features of gluino signal events satisfying our selection criteria for our natural SUSY benchmark point

with $m_{\tilde{g}} \simeq 2$ TeV and $m_{\tilde{t}_1} \sim 1500$ GeV. Figure 6 shows the transverse energy distribution of the four hardest jets from the two tagged b -jet signal as well as from the backgrounds, after the cut set (7). We see that the two hardest jets typically have $E_T \sim 700$ and 400 GeV, respectively, while the third and fourth jet E_T distributions peak just below 300 and 200 GeV. The distributions for the signal with three tagged b -jets are very similar and not shown for brevity. While the actual peak positions in the distributions depend on the gluino and stop masses, the fact that the events contain four hard jets is rather generic. We also see that the SM background after these cuts is negligibly small, and that we do indeed have a pure sample of gluino events.

In Fig. 7, we show the jet multiplicity for the benchmark point signal and background events after our selection cuts for both the two tagged b -jet (solid) and the three tagged b -jet (dashed) samples. Recall that jets are defined to be hadronic clusters with $E_T > 50$ GeV. We see that the signal indeed has

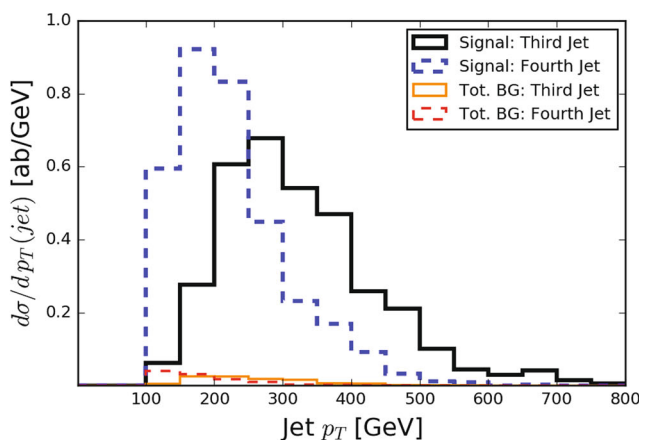
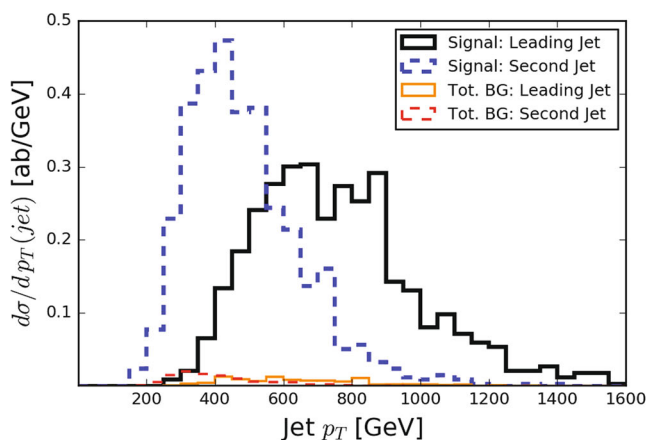


Fig. 6 Transverse momenta of the leading jet and second-leading jet in p_T (left) and for the third and fourth-leading jets (right) for signal and background events after 2b analysis cuts. The distribution of these quantities after 3b analysis cuts is similar

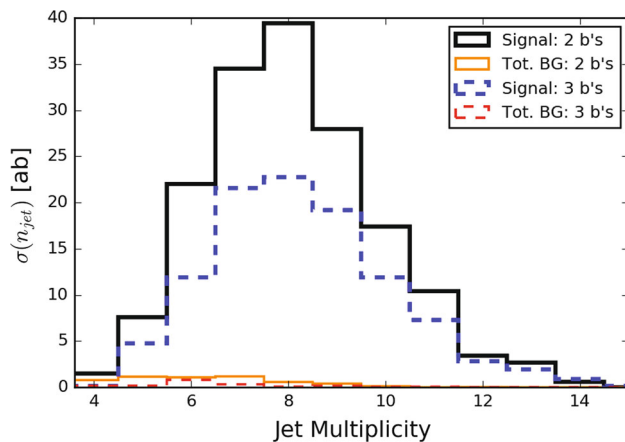


Fig. 7 Jet multiplicity for signal and background events satisfying our 2b and 3b analysis cuts. Recall that we require jets to have $p_T > 50$ GeV and $|\eta| < 3.0$

very high jet multiplicity relative to the background. Since the exact jet multiplicity may be sensitive to details of jet definition, and because our simulation of the background with very high jet multiplicity is less reliable due to the use of the shower approximation rather than exact matrix elements, we have *not used* jet-multiplicity cuts to further enhance the signal over background. (Note: the sum of cross sections above a minimum jet multiplicity, as implemented in the **C1** cuts, is not expected to depend much on the implementation of the jet-multiplicity cut.)

In Fig. 8 we show the transverse momentum of b -tagged jets in signal and background events satisfying the final cuts for ≥ 2 tagged b -jet events (left frame) and for ≥ 3 tagged b -jet events (right frame). We see that the hardest b -jet E_T ranges up to ~ 1 TeV, while the second b -jet, for the most part, has $E_T \sim 100$ – 600 GeV. Again, we stress that the b -jet spectrum shape will be somewhat sensitive to the gluino–stop as well as stop–higgsino mass differences, but the hardness of the b -jets is quite general. We expect that the b -jets would remain hard (though the E_T distributions would have different shapes) even in the case when the stop is heavier than the gluino, and the gluino instead dominantly decays via the three body modes, $\tilde{g} \rightarrow t\bar{t}\tilde{Z}_{1,2}$ and $\tilde{g} \rightarrow tb\tilde{W}_1$.

Before turning to a discussion of our results for the mass reach and of the feasibility of the extraction of $m_{\tilde{g}}$ using the very pure sample of signal events, we address the sensitivity of our cross section calculations to the Isajet b -tagging efficiency and purity algorithm that we have used. This algorithm was based on early ATLAS studies [81,82] of WH and $t\bar{t}H$ processes where the transverse momentum of the b -jets is limited to several hundred GeV. More recently, the CMS Collaboration [85] has provided loose, medium and tight b -tagging algorithms with corresponding charm and light parton mis-tags whose validity extends out to a TeV. We show a comparison of the SUSY signal rate for our SUSY bench-

mark point for the sample with at least two/three tagged b -jets after the selection cuts (7)/(8) in Table 3. We illustrate results for the medium and tight algorithms in Ref. [85]. Also shown, in parentheses are the corresponding signal-to-background ratios, after these cuts. We see that the cross sections for the Isajet parametrization of the b -tagging efficiency, as well as the corresponding values of S/B lie between those obtained using the medium and tight algorithms in the recent CMS study. Although it is difficult to project just how well b -tagging will perform in the high-luminosity environment, we are encouraged to see that our simple algorithm gives comparable answers to those obtained using the more recent tagging algorithms in Ref. [85] even though we have very hard b -jets in the signal.

5 Results

In this section, we show that the pure sample of gluino events that we have obtained can be used to make projections for both the gluino mass reach and for the extraction of the gluino mass, along the RNS model line introduced at the start of Sect. 2. We consider several values of integrated luminosities at LHC14 ranging from 150fb^{-1} to the 3000fb^{-1} projected to be accumulated at the high-luminosity LHC.

5.1 Gluino mass reach

We begin by showing in Fig. 9 the gluino signal cross section after all analysis cuts via both the ≥ 2 tagged b -jets (left frame) and the ≥ 3 tagged b -jets (right frame) channels. The total SM backgrounds in these channels are 5.3 ab and 1.8 ab, respectively. The various horizontal lines show the minimum cross section for which a Poisson fluctuation of the expected background occurs with a Gaussian probability corresponding to 5σ , for several values of integrated luminosities at LHC14, starting with 150fb^{-1} expected (per experiment) before the scheduled 2018 LHC shutdown, 300fb^{-1} the anticipated design integrated luminosity of LHC14, as well as 1ab^{-1} and 3ab^{-1} , which are expected to be accumulated after the high-luminosity upgrade of the LHC. We have checked that for an observable signal we always have a minimum of five events and a sizable signal-to-background ratio. (The lowest value for signal-to-background ratio we consider, i.e., the value at the maximum gluino mass for which we have 5σ discovery with at least five events is for 3000fb^{-1} in our 2b analysis, for which $S/B = 1.6$.) We see from Fig. 9 that, with 150fb^{-1} , LHC experiments would be probing $m_{\tilde{g}}$ values up to 2300 GeV (actually somewhat smaller since the machine energy is still 13 TeV) via the 2b analysis, with only a slightly smaller reach via the 3b analysis. Even for the decoupled squark scenario, we project a 3000fb^{-1} LHC14 5σ gluino reach to ~ 2400 GeV; this will

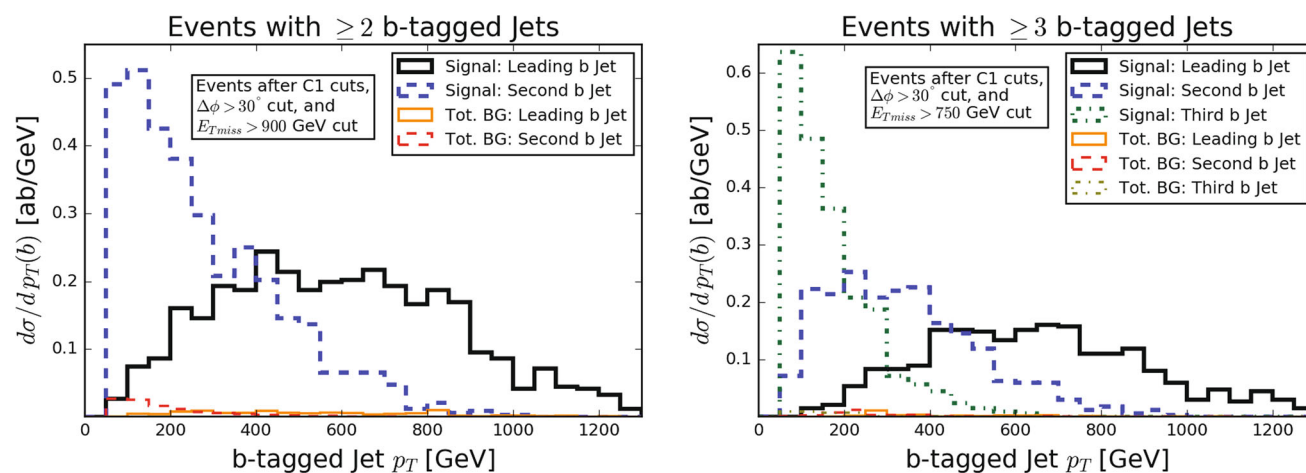


Fig. 8 The distribution of the transverse momenta of the leading and second-leading b -tagged jet after (left) the 2b analysis cuts and (right) the 3b analysis cuts

Table 3 The LHC signal cross section in ab for our SUSY benchmark point for ≥ 2 tagged b -jet events, and for ≥ 3 tagged b -jet events after all the analysis cuts in (7) and (8), respectively. The numbers in parenthe-

ses are the corresponding signal-to-background ratios. We show results for the Isajet parametrization of b -tagging efficiency as well as for the medium and tight b -tagging efficiencies in Ref. [85]

| | Isajet | CMS medium | CMS tight |
|--|----------|------------|-----------|
| ≥ 2 tagged b jets, $\cancel{E}_T > 900$ GeV | 167 (32) | 207 (25) | 121 (39) |
| ≥ 3 tagged b jets, $\cancel{E}_T > 750$ GeV | 105 (59) | 182 (47) | 61.1 (78) |

extend to about 2800 GeV in both the 2b and the 3b channels at the HL-LHC. These projections are significantly greater than the corresponding reach from the mSUGRA model [97] because: (1) the presence of hard b -jets in the signal serves as an additional handle to reduce SM backgrounds, especially those from W, Z +jet production processes [98–100], and (2) the larger $m_{\tilde{g}} - m_{\tilde{z}_1}$ mass gap expected from RNS leads to harder jets and harder \cancel{E}_T as compared to mSUGRA. A further improvement in reach may of course be gained by combining ATLAS and CMS data sets.

5.2 Gluino mass measurement

We now turn to the examination of whether the clean sample of gluino events that we have obtained allows us to extract the mass of the gluino. For decoupled first/second generation squarks, these events can only originate via gluino pair production. Assuming that the background is small, or can be reliably subtracted, the event rate is completely determined by $m_{\tilde{g}}$. A determination of this event rate after the analysis cuts in (7) or (8) should, in principle, yield a measure of the gluino mass.

Our procedure for the extraction of the gluino mass (for our benchmark point) is illustrated in the left frame of Fig. 10, where we show a blow-up of the SUSY signal cross section versus $m_{\tilde{g}}$ for ≥ 2 tagged b -jet events after all our analysis cuts. The signal cross section can be inferred from the

observed number of events in the sample and subtracting the expected background. The error bar shown in the figure is obtained by combining in quadrature the 1σ statistical error on the cross section based on the expected total number of (signal plus background) events expected in the sample, with a 15% theoretical error on the gluino production cross section.⁴ This error bar is used to project “the 1σ ” uncertainty in the measurement of $m_{\tilde{g}}$. From the figure, $m_{\tilde{g}} = 2000^{+80}_{-70}$ GeV with 150 fb^{-1} , and $m_{\tilde{g}} = (2000^{+50}_{-45})$ GeV with 3 ab^{-1} . The right frame of Fig. 10 shows the precision with which the gluino mass may be extracted via the clean events in the ≥ 2 tagged b -jets channel versus the gluino mass for four different values of integrated luminosity ranging from 150 fb^{-1} to 3 ab^{-1} . The shading on the various bands extends out to

⁴ The LHC SUSY Cross Section Working Group [101, 102] currently cites a theoretical error of $\sim 30\%$. (The quoted error is 29.1% for a gluino mass of 2 TeV and rises with mass; for $m_{\tilde{g}} = 2.6 \text{ TeV}$ the error is 40.8%.) This error includes uncertainties in the relevant parton distribution functions (pdfs) as well as the estimate of the contribution from uncalculated higher order diagrams indicated by the variation of the renormalization and factorization scales. We project that this error will be reduced by a factor of 2 by the time the high-luminosity LHC is operational, as pdfs will be better known and even higher order contributions will have been calculated. We have checked that the precision on the gluino mass changes by only $\gtrsim 1\%$ if we assume a 30% theory error instead of a 15% theory error. As an example the larger 1σ error bar changes from 4.8 to 6.2% for the maximum discoverable gluino mass ($\sim 2400 \text{ GeV}$) with 300 fb^{-1} of integrated luminosity.

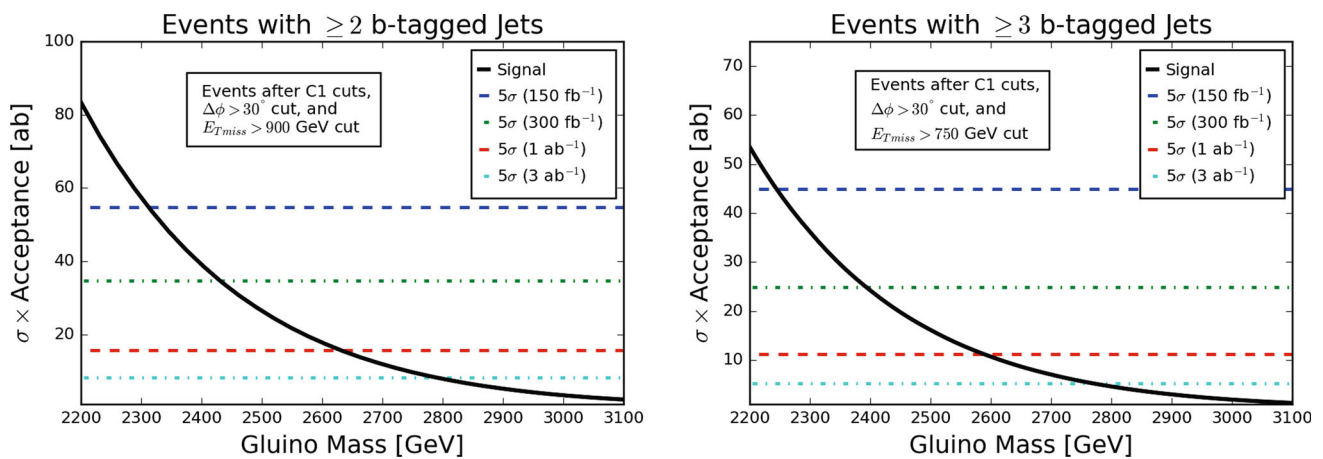


Fig. 9 The gluino signal cross section for the ≥ 2 tagged b -jet (left) and the ≥ 3 tagged b -jet channels (right) after all the analysis cuts described in the text. The horizontal lines show the minimum cross section for which the Poisson fluctuation of the corresponding SM background lev-

els, 5.3 ab for 2b events and 1.8 ab for 3b events, occurs with a Gaussian probability corresponding to 5σ for integrated luminosities for several values of integrated luminosities at LHC14

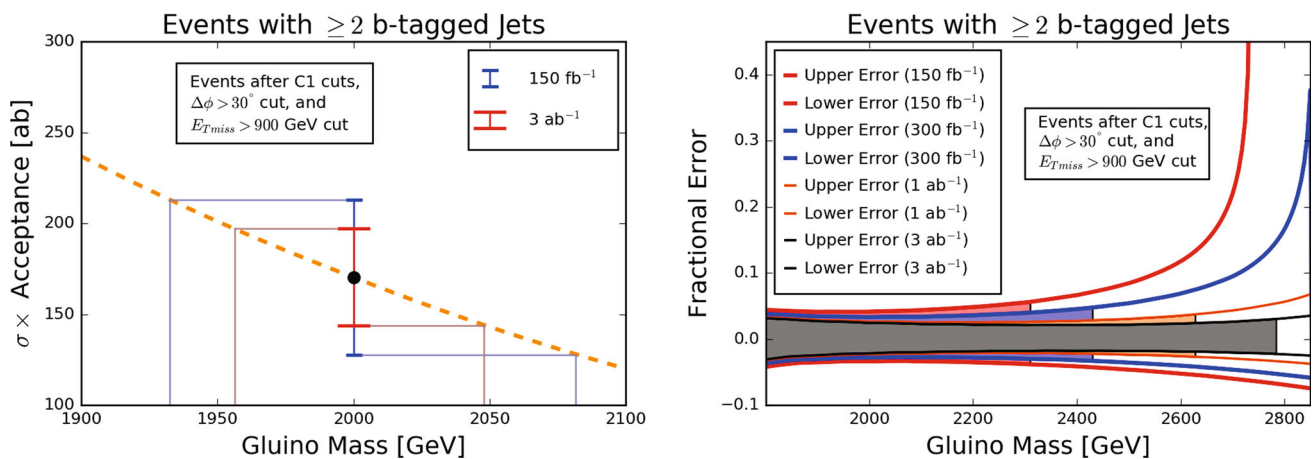


Fig. 10 Illustration of our method to extract the precision with which the gluino mass may be extracted at the LHC for the 2b sample (left frame) and the statistical precision that may be attained as a function of $m_{\tilde{g}}$ for integrated luminosities of 150 fb^{-1} , 300 fb^{-1} , 1 ab^{-1} and 3 ab^{-1} (right frame). The left frame shows a blow-up of the gluino signal cross section versus $m_{\tilde{g}}$ for the ≥ 2 tagged b -jets after all the analysis cuts described in the text. Also shown are the “ 1σ ” error bars for a determination of this cross section (where the 1σ statistical error on the observed number of signal events and a 15% uncertainty on the gluino production

cross section have been combined in quadrature) for an integrated luminosity of 150 fb^{-1} (blue) and 3 ab^{-1} (red). The other lines show how we obtain the precision with which the gluino mass may be extracted for our benchmark gluino point for these two values of integrated luminosities. The bands in the right frame illustrate the statistical precision on the extracted value of $m_{\tilde{g}}$ that may be attained at the LHC for four different values of integrated luminosity. We terminate the shading at the 5σ discovery reach shown in Fig. 9

the 5σ reach projection in Fig. 9. We see that gluino mass extraction with a sub-ten percent precision is possible with even 150 fb^{-1} of integrated luminosity if gluinos are lighter than 2.5 TeV and cascade decay via stops into light higgsinos as in the RNS framework. It should be noted though that the 5σ reach of the LHC extends to just ~ 2.3 TeV so that the determination, $m_{\tilde{g}} = 2.5$ TeV would be a mass measurement for a discovery with a significance smaller than the customary 5σ . At the high-luminosity LHC, the gluino mass may be extracted with a statistical precision better than 2–5%

(depending on their mass) all the way up to $m_{\tilde{g}} \sim 2.8$ TeV, i.e., if gluinos are within the 5σ discovery range of the HL–LHC! Gluino mass determination would also be possible for the range of gluino masses for which the discovery significance was smaller than 5σ .

Prospects for gluino mass measurement via the ≥ 3 tagged b -jet sample are shown in Fig. 11. We see that the statistical precision on the mass measurement that may be attained is somewhat worse than that via the $\geq 2b$ channel shown in Fig. 10, though not qualitatively different except at the high

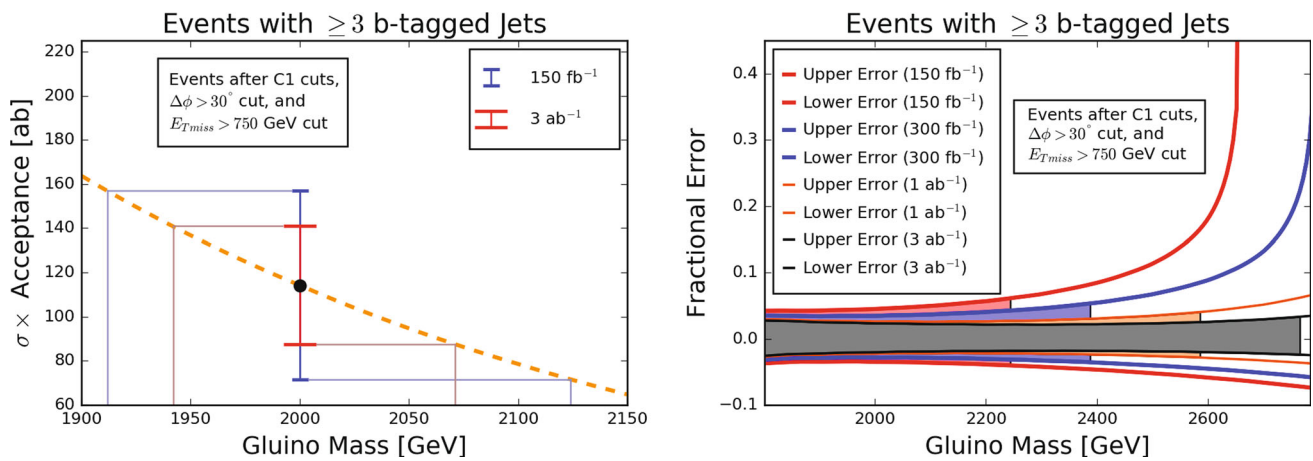


Fig. 11 The same as Fig. 10, but for the clean SUSY sample with ≥ 3 tagged b -jets

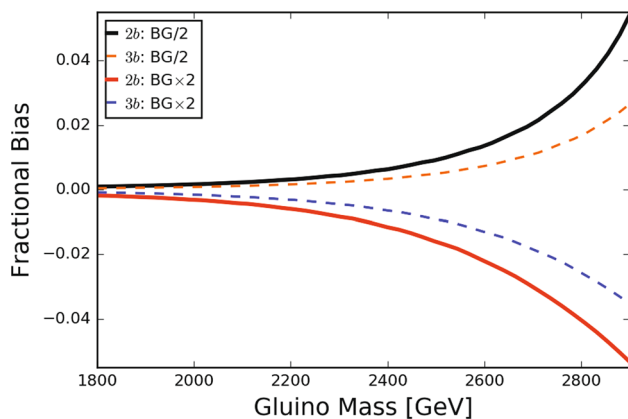


Fig. 12 The systematic bias, discussed in the text, in the measurement of the gluino mass resulting from a mis-estimate of the SM background by a factor of 2 in either direction. The *solid lines* are for the signal in the 2b channel while the *dashed lines* are for the signal in the 3b channel

mass end. The difference is, of course, due to the lower event rate in this channel.

Before proceeding further, we point out that in order to extract the gluino mass, we have assumed that our estimate of the background is indeed reliable. Since the expected background has to be subtracted from the observed event rate to obtain the signal cross section, and via this the value of $m_{\tilde{g}}$, any error in the estimation of the expected background will result in a *systematic shift* in the extracted gluino mass. For instance, an over-estimation of the background expectation compared to its true value, will result in too small a signal and a corresponding overestimate of the mass of the gluino. We expect that by the time a precise mass measurement becomes feasible, it will be possible to extract the SM background to a good precision by extrapolating the backgrounds normalized in the “background region” (which are expected to have low signal contamination) to the “signal region” using the accumulated data.

We show in Fig. 12 the systematic bias on the gluino mass that could result because the background estimate differs from the true value by a factor of 2. We see that this (asymmetric) systematic bias is below 2% for $m_{\tilde{g}} \lesssim 2.6$ TeV, but becomes as large as 4% for the largest masses for which there is a 5σ signal at the high-luminosity LHC in the two tagged b -jets sample. This bias is smaller for the three tagged b -jets sample because the corresponding background is smaller.

Before closing this discussion, we should mention that stop pair contamination to the gluino sample will not qualitatively alter our conclusions regarding the feasibility of the gluino mass extraction using the total rate (or regarding the discovery prospects for the gluino). Toward this end, we have determined that after our selection cuts, stop pair production contributes 15 ab, 7 ab and 0.8 ab for $m_{\tilde{t}_1} = 1, 1.5$ and 2 TeV, respectively in the ≥ 2 tagged b -case to be compared with a signal cross section of ~ 27 ab for $m_{\tilde{g}} = 2.5$ TeV and a background cross section of 5 ab. We have also checked that by requiring H_T (the scalar sum of the E_T of all jets and leptons along with \cancel{E}_T) $\gtrsim 3$ TeV, the bulk of the stop contribution is eliminated for $m_{\tilde{t}_1} = 1$ TeV [reduced by about 50%, for $m_{\tilde{t}_1} = 1.5$ TeV], with only a very modest loss of signal if $m_{\tilde{g}} > 2.5$ TeV.⁵ We thus conclude that stop pair production will not significantly degrade the precision with which we will be able to extract $m_{\tilde{g}}$ using the total rate. For the ≥ 3 tagged b -jet sample, the stop contamination is lower by a factor of 2.5–8, depending on the stop mass and so even less of a problem.

The reader may be concerned that our mass extraction based on the event rate is contingent upon our assumption that the gluinos always decay via $\tilde{g} \rightarrow \tilde{t}_1 t$ and the \tilde{t}_1 always decays to higgsinos. This decay pattern is expected in natural SUSY models with unified gaugino masses. While this may

⁵ It should also be noted that HL–LHC experiments will be able to discover \tilde{t}_1 if $m_{\tilde{t}_1} < 1.4$ TeV [97].

appear model-dependent, we stress that there must simultaneously be other signals (already mentioned in Sect. 1) present at the HL-LHC that would serve to validate that we are indeed within the RNS framework introduced in Sect. 2 (where gluinos and stops decay as expected). These include 1. the same-sign $W^\pm W^\pm + \cancel{E}_T$ signal from gaugino pair production that leads to same-sign lepton pair production events with modest jet activity (only from initial state QCD radiation [52]), as well as 2. monojet events with low mass, soft opposite-sign dileptons [53–56]. Higgsino production may also be observable at an electron–positron linear collider if such a facility is built and higgsinos are kinematically accessible. The assumed dominance of gluino decays to top squarks will also likely be testable from the b -jet multiplicity in multi-jet plus \cancel{E}_T events:⁶ if gluinos have substantial branching fractions to first and second generation squarks, squark pair production and associated gluino squark production can be substantial, and the rate for multi-jet plus \cancel{E}_T events (but without b -tags) will be correspondingly larger than in our scenario.

Our conclusions for the precision with which LHC measurements might extract the gluino mass are very striking, and we should temper these with some cautionary remarks. The most important thing is that any extraction of the mass from the absolute event rate assumes an excellent understanding of the detector in today’s environment as well as in the high-luminosity environment of future experiments. While we are well aware that our theorists’ simulation does not include many important effects, e.g., particle detection efficiencies, jet energy scales, full understanding of b -tagging efficiencies particularly for very high E_T b -jets, to name a few, we are optimistic that these will all be very well understood (given that there will be a lot of data) by the time gluino mass measurements become feasible. The fact that our proposal relies on an inclusive cross section with ≥ 4 jets (of which 2 or 3 are b -jets) and does not entail very high jet multiplicities suggests that our procedure should be relatively robust. An excellent understanding of the \cancel{E}_T tail from SM sources, as well as of the tagging efficiency (and associated purity) for very high E_T b -jets are crucial elements for this analysis.

6 Summary

In this paper, we have re-examined LHC signals from the pair production of gluinos assuming gluinos decay via $\tilde{g} \rightarrow t\tilde{t}_1$, followed by stop decays, $\tilde{t}_1 \rightarrow b\tilde{W}_1, t\tilde{Z}_{1,2}$, to higgsinos, where the visible decay products of the higgsinos are very soft. This is the dominant gluino decay chain expected within the radiatively-driven natural SUSY framework that we have

suggested for phenomenological analysis of simple natural SUSY GUT models. For our analysis, we have used the RNS model line detailed in Sect. 2 with higgsino masses ~ 150 GeV. The gluino signal then consists of events with ≥ 4 hard jets, two or three of which are tagged as b -jets together with very large \cancel{E}_T . We expect that our results are only weakly sensitive to our choice of higgsino mass as long as the electroweak fine-tuning parameter $\Delta_{EW} \lesssim 30$.

The new features that we have focused on in this analysis are the very large data sets ($300\text{--}3000 \text{ fb}^{-1}$) that are expected to be available at the LHC and its high-luminosity upgrade and the capability for tagging very hard b -jets with E_T up to a TeV and beyond. We have identified a set of very stringent cuts, detailed in (7) and (8), that allows us to isolate the gluino signal from SM backgrounds: our procedure yields a signal-to-background ratio >30 (>60) in the two (three) tagged b -jets channel for $m_{\tilde{g}} = 2$ TeV, and >3 (>6) for $m_{\tilde{g}} = 2.6$ TeV. Even for decoupled squarks, these relatively pure data samples extend the gluino discovery reach in the RNS framework to 2.4 TeV for an integrated luminosity of 300 fb^{-1} expected by end of the current LHC run, and to 2.8 TeV with 3000 fb^{-1} anticipated after the luminosity upgrade of the LHC. These may be compared to projections [97] for the gluino reach of 1.8 TeV (2.3 TeV) for 300 fb^{-1} (3000 fb^{-1}) within the mSUGRA/CMSSM framework. We attribute the difference to: (1) the presence of b -jets in the signal which serve to essentially eliminate SM backgrounds from V +jet production, and also reduce those from other sources and (2) the comparatively harder jet E_T and \cancel{E}_T spectrum associated with RNS models.

The separation of a relatively clean gluino sample also allows a determination of the gluino mass based on the *signal event rate* rather than kinematic properties of the event. Although the determination of the mass from the event rate hinges upon being able to predict the absolute normalization of the expected signal after cuts, and so requires an excellent understanding of the detector, we are optimistic that LHC experimenters will be able to use the available data to be able to reliably determine acceptances and efficiencies in the signal region by the time these measurements become feasible. We project that with 300 fb^{-1} of integrated luminosity, experiments at LHC14 should be able to measure $m_{\tilde{g}}$ with a 1σ statistical error of $<4.8\%$ for $m_{\tilde{g}} = 2.4$ TeV, i.e., all the way up to its 5σ discovery limit. At the high-luminosity LHC, the projected precision for a gluino mass measurement ranges between about 2.5% for $m_{\tilde{g}} = 2$ TeV to about 3% near its 5σ discovery limit of 2.8 TeV in the ≥ 2 tagged b -jet channels. Comparable precision is obtained also via the ≥ 3 tagged b channel. In this connection, we should also keep in mind that a factor of 2 uncertainty in the projected background will result in a small (but not negligible) systematic uncertainty ranging between $\lesssim 1\%$ for $m_{\tilde{g}} < 2400$ GeV to about 4% for

⁶ By the time these measurements become possible, b -jet tagging at the LHC will be very well understood.

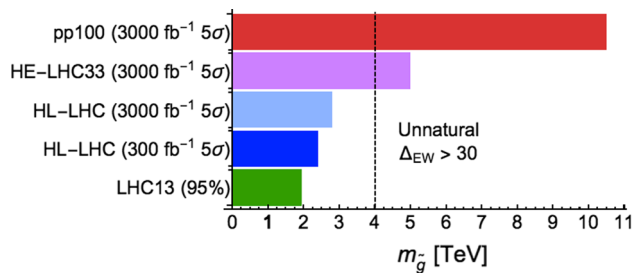


Fig. 13 The approximate reach for various present and future hadron collider options for gluino pair production. The region to the right of the dashed line yields large electroweak fine-tuning and is considered unnatural

$m_{\tilde{g}} = 2800$ GeV in the extraction of $m_{\tilde{g}}$ via the ≥ 2 tagged b channel and smaller than this for the ≥ 3 tagged b channel.

An observation of a SUSY signal in both the 2b and the 3b channels, and the extraction of a common value of $m_{\tilde{g}}$ would certainly be strong evidence for a discovery of a new particle. If these signals are accompanied by other signals such as the same-sign diboson signal and/or monojet events with soft opposite-sign dileptons, the case for the discovery of radiatively-driven natural SUSY would be very strong. In this case, depending on the gluino mass, there may also be signals in trilepton and even four lepton plus jets plus E_T channels [50].

In Fig. 13 we compare the approximate reach for various present and future hadron collider options for gluino pair production. The region to the right of the dashed line yields large electroweak fine-tuning and is considered unnatural. The green bar shows the present LHC 95% CL limit on $m_{\tilde{g}}$ as derived in several simplified models which should be applicable to the present RNS case. The dark and light blue bars show our projected LHC14 300 and 3000 fb^{-1} 5σ reaches for RNS. These cover only a portion of natural SUSY parameter space. The lavender bar shows the reach of HE-LHC with $\sqrt{s} = 33$ TeV as abstracted from Ref. [103] where it is assumed that the gluino directly decays to a light LSP via $\tilde{g} \rightarrow q\bar{q}\tilde{Z}_1$ (presumably with no enhancement of decays to third generation quarks). The 5σ HE-LHC for 3000 fb^{-1} extends to $m_{\tilde{g}} \sim 5$ TeV and thus covers all of natural SUSY parameter space. The red bar shows the corresponding gluino reach of a 100 TeV pp collider at 5σ and 3000 fb^{-1} , as taken also from Ref. [103]. Here, the reach extends just beyond $m_{\tilde{g}} \sim 10$ TeV. It probes only more deeply into unnatural SUSY parameter space beyond the complete coverage of the gluino offered by HE-LHC, but does offer the possibility of a squark discovery.

In summary, in models such as RNS where gluinos dominantly decay via $\tilde{g} \rightarrow t\tilde{t}_1$, and the stops decay to light higgsinos via $\tilde{t}_1 \rightarrow \tilde{W}_1 b, \tilde{Z}_{1,2} t$, signals from gluino pair production should be observable at the 5σ level out to $m_{\tilde{g}} < 2.4$ (2.8) TeV for an integrated luminosity of 300 fb^{-1}

(3000 fb^{-1}) in the ≥ 4 -jet sample with very hard E_T and two or three tagged b -jets. The clean sample of gluino events that we obtain should also allow a measurement of $m_{\tilde{g}}$ with a statistical precision ranging from 2–5% depending on the gluino mass and the assumed integrated luminosity, ranging between 300–3000 fb^{-1} , along with a smaller but non-negligible systematic uncertainty of 1–4% mentioned in the previous paragraph. The precision of gluino mass extraction should be even greater using the combined ATLAS/CMS data set.

Acknowledgements We thank Heather Gray, Jacobo Konigsberg, Bill Murray, Markus Klute and Giacomo Polesello for helpful discussions as regards b -jet tagging at the LHC and we thank P. Skubic for reading the manuscript. This work was supported in part by the US Department of Energy, Office of High Energy Physics, and was aided by the use of SLAC Computing Resources and the LHCO_reader Python package [104]. JG would like to express a special thanks to the Mainz Institute for Theoretical Physics (MITP) for its hospitality and support. VB thanks the KITP at University of California-Santa Barbara for hospitality. This research was supported in part by the National Science Foundation under Grant No. NSF PHY11-25915.

Open Access This article is distributed under the terms of the Creative Commons Attribution 4.0 International License (<http://creativecommons.org/licenses/by/4.0/>), which permits unrestricted use, distribution, and reproduction in any medium, provided you give appropriate credit to the original author(s) and the source, provide a link to the Creative Commons license, and indicate if changes were made. Funded by SCOAP³.

References

1. E. Witten, Nucl. Phys. B **188**, 513 (1981)
2. R.K. Kaul, Phys. Lett. B **109**, 19 (1982)
3. S. Dimopoulos, S. Raby, F. Wilczek, Phys. Rev. D **24**, 1681 (1981)
4. U. Amaldi, W. de Boer, H. Furstenau, Phys. Lett. B **260**, 447 (1991)
5. J.R. Ellis, S. Kelley, D.V. Nanopoulos, Phys. Lett. B **260**, 131 (1991)
6. P. Langacker, M.X. Luo, Phys. Rev. D **44**, 817 (1991)
7. L.E. Ibañez, G.G. Ross, Phys. Lett. B **110**, 215 (1982)
8. K. Inoue et al., Prog. Theor. Phys. **68**, 927 (1982)
9. K. Inoue et al., Prog. Theor. Phys. **71**, 413 (1984)
10. L. Ibañez, Phys. Lett. B **118**, 73 (1982)
11. H.P. Nilles, M. Srednicki, D. Wyler, Phys. Lett. B **120**, 346 (1983)
12. J. Ellis, J. Hagelin, D. Nanopoulos, M. Tamvakis, Phys. Lett. B **125**, 275 (1983)
13. L. Alvarez-Gaumé, J. Polchinski, M. Wise, Nucl. Phys. B **221**, 495 (1983)
14. B.A. Ovrut, S. Raby, Phys. Lett. B **130**, 277 (1983)
15. L.E. Ibanez, G.G. Ross, C. R. Phys. **8**, 1013 (2007)
16. G. Aad et al. [ATLAS Collaboration], Phys. Lett. B **716**, 1 (2012)
17. S. Chatrchyan et al. [CMS Collaboration], Phys. Lett. B **716**, 30 (2012)
18. H.E. Haber, R. Hempfling, Phys. Rev. Lett. **66**, 1815 (1991)
19. J.R. Ellis, G. Ridolfi, F. Zwirner, Phys. Lett. B **257**, 83 (1991)
20. Y. Okada, M. Yamaguchi, T. Yanagida, Prog. Theor. Phys. **85**, 1 (1991)
21. M.S. Carena, H.E. Haber, Prog. Part. Nucl. Phys. **50**, 63 (2003). [arXiv:hep-ph/0208209](https://arxiv.org/abs/hep-ph/0208209)

22. G. Aad et al. [ATLAS Collaboration], JHEP **1409**, 176 (2014)
23. G. Aad et al. [ATLAS Collaboration], JHEP **1504**, 116 (2015)
24. CMS Collaboration [CMS Collaboration], CMS-PAS-SUS-14-011
25. The ATLAS collaboration, ATLAS-CONF-2015-067
26. W. Adam, Plenary talk presented at the 38th *International Conference on High Energy Physics*, Chicago, USA (Aug. 2016)
27. The ATLAS collaboration [ATLAS Collaboration], ATLAS-CONF-2016-052
28. R. Barbieri, G.F. Giudice, Nucl. Phys. B **306**, 63 (1988)
29. J.R. Ellis, K. Enqvist, D.V. Nanopoulos, F. Zwirner, Mod. Phys. Lett. A **1**, 57 (1986)
30. H. Baer, V. Barger, M. Savoy, Phys. Rev. D **93**(3), 035016 (2016)
31. G. Aad et al. [ATLAS Collaboration], JHEP **1411**, 118 (2014)
32. S. Chatrchyan et al. [CMS Collaboration], Eur. Phys. J. C **73**(12), 2677 (2013)
33. S. Dimopoulos, G.F. Giudice, Phys. Lett. B **357**, 573 (1995)
34. M. Papucci, J.T. Ruderman, A. Weiler, JHEP **1209**, 035 (2012)
35. C. Brust, A. Katz, S. Lawrence, R. Sundrum, JHEP **1203**, 103 (2012)
36. J. Lykken, M. Spiropulu, Sci. Am. **310N5**, 36 (2014)
37. A. Strumia, JHEP **1104**, 073 (2011)
38. N. Craig, [arXiv:1309.0528](https://arxiv.org/abs/1309.0528)
39. M. Dine, Ann. Rev. Nucl. Part. Phys. **65**, 43 (2015)
40. H. Baer, V. Barger, P. Huang, A. Mustafayev, X. Tata, Phys. Rev. Lett. **109**, 161802 (2012)
41. H. Baer, V. Barger, P. Huang, D. Mickelson, A. Mustafayev, X. Tata, Phys. Rev. D **87**(11), 115028 (2013)
42. H. Baer, V. Barger, D. Mickelson, Phys. Rev. D **88**, 095013 (2013)
43. A. Mustafayev, X. Tata, Indian J. Phys. **88**, 991 (2014)
44. H. Baer, V. Barger, D. Mickelson, M. Padeffke-Kirkland, Phys. Rev. D **89**, 115019 (2014)
45. H. Baer, V. Barger, M. Savoy, Phys. Scripta **90**, 068003 (2015). doi:[10.1088/0031-8949/90/6/068003](https://doi.org/10.1088/0031-8949/90/6/068003)
46. H. Baer, V. Barger, M. Savoy, Phys. Rev. D **93**(7), 075001 (2016)
47. H. Baer, V. Barger, A. Mustafayev, Phys. Rev. D **85**, 075010 (2012)
48. H. Baer, X. Tata, J. Woodside, Phys. Rev. D **42**, 1568 (1990)
49. H. Baer, C.H. Chen, M. Drees, F. Paige, X. Tata, Phys. Rev. D **58**, 075008 (1998)
50. H. Baer, V. Barger, P. Huang, D. Mickelson, A. Mustafayev, W. Sreethawong, X. Tata, JHEP **1312**, 013 (2013)
51. B. Altunkaynak, H. Baer, V. Barger, P. Huang, Phys. Rev. D **92**(3), 035015 (2015)
52. H. Baer, V. Barger, P. Huang, D. Mickelson, A. Mustafayev, W. Sreethawong, X. Tata, Phys. Rev. Lett. **11015**, 151801 (2013)
53. Z. Han, G. D. Kribs, A. Martin, A. Menon, Phys. Rev. D **89**(7), 075007 (2014)
54. H. Baer, A. Mustafayev, X. Tata, Phys. Rev. D **90**(11), 115007 (2014)
55. C. Han, D. Kim, S. Munir, M. Park, JHEP **1504**, 132 (2015)
56. H. Baer, V. Barger, M. Savoy, X. Tata, Phys. Rev. D **94**, 035025 (2016)
57. H. Baer, V. Barger, D. Mickelson, A. Mustafayev, X. Tata, JHEP **1406**, 172 (2014)
58. H. Baer, M. Berggren, K. Fujii, S.L. Lehtinen, J. List, T. Tanabe, J. Yan, PoS ICHEP **2016**, 156 (2016). [arXiv:1611.02846](https://arxiv.org/abs/1611.02846) [hep-ph]
59. H. Baer, V. Barger, M. Padeffke-Kirkland, X. Tata, Phys. Rev. D **89**, 037701 (2014)
60. H. Baer, V. Barger, G. Shaughnessy, H. Summy, L.T. Wang, Phys. Rev. D **75**, 095010 (2007)
61. W.S. Cho, K. Choi, Y.G. Kim, C.B. Park, Phys. Rev. Lett. **100**, 171801 (2008)
62. M.M. Nojiri, Y. Shimizu, S. Okada, K. Kawagoe, JHEP **0806**, 035 (2008)
63. K. Agashe, R. Franceschini, D. Kim, JHEP **1411**, 059 (2014)
64. M. Burns, K. Kong, K.T. Matchev, M. Park, JHEP **0903**, 143 (2009)
65. W.S. Cho et al., JHEP **1408**, 070 (2014)
66. D. Matalliotakis, H.P. Nilles, Nucl. Phys. B **435**, 115 (1995)
67. P. Nath, R.L. Arnowitt, Phys. Rev. D **56**, 2820 (1997)
68. J. Ellis, K. Olive, Y. Santoso, Phys. Lett. B **539**, 107 (2002)
69. J. Ellis, T. Falk, K. Olive, Y. Santoso, Nucl. Phys. B **652**, 259 (2003)
70. H. Baer, A. Mustafayev, S. Profumo, A. Belyaev, X. Tata, JHEP **0507**, 065 (2005)
71. H. Baer, F. Paige, S. Protopopescu, X. Tata, ISAJET. [arXiv:hep-ph/0312045](https://arxiv.org/abs/hep-ph/0312045)
72. W. Beenakker, R. Hopker, M. Spira, P.M. Zerwas, Nucl. Phys. B **492**, 51 (1997). doi:[10.1016/S0550-3213\(97\)80027-2](https://doi.org/10.1016/S0550-3213(97)80027-2). [arXiv:hep-ph/9610490](https://arxiv.org/abs/hep-ph/9610490)
73. W. Beenakker, S. Brensing, M.N. Kramer, A. Kulesza, E. Laenen, L. Motyka, I. Niessen, Int. J. Mod. Phys. A **26**, 2637 (2011). doi:[10.1142/S0217751X11053560](https://doi.org/10.1142/S0217751X11053560). [arXiv:1105.1110](https://arxiv.org/abs/1105.1110) [hep-ph]
74. K.J. Bae, H. Baer, E.J. Chun, Phys. Rev. D **89**(3), 031701 (2014)
75. K.J. Bae, H. Baer, E.J. Chun, JCAP **1312**, 028 (2013)
76. K.J. Bae, H. Baer, A. Lessa, H. Serce, JCAP **1410**(10), 082 (2014)
77. J. Alwall, M. Herquet, F. Maltoni, O. Mattelaer, T. Stelzer, JHEP **1106**, 128 (2011)
78. J. Alwall, R. Frederix, S. Frixione, V. Herschi, F. Maltoni, O. Mattelaer, H.-S. Shao, T. Stelzer, P. Torrielli, M. Zaro, JHEP **1407**, 079 (2014)
79. T. Sjostrand, S. Mrenna, P.Z. Skands, Comput. Phys. Commun. **178**, 852 (2008)
80. J. de Favereau et al. [DELPHES 3 Collaboration], JHEP **1402**, 057 (2014)
81. S. Corradé, V. Kostoukine, J. Levêque, A. Rozanov, J.B. de Vivie, ATLAS Note, ATLAS-PHYS-2004-006
82. V. Kostoukine, ATLAS Note, ATLAS-PHYS-2003-033
83. M. Cacciari, G.P. Salam, G. Soyez, JHEP **0804**, 063 (2008). doi:[10.1088/1126-6708/2008/04/063](https://doi.org/10.1088/1126-6708/2008/04/063). [arXiv:0802.1189](https://arxiv.org/abs/0802.1189) [hep-ph]
84. M. Cacciari, G.P. Salam, G. Soyez, Eur. Phys. J. C **72**, 1896 (2012). doi:[10.1140/epjc/s10052-012-1896-2](https://doi.org/10.1140/epjc/s10052-012-1896-2). [arXiv:1111.6097](https://arxiv.org/abs/1111.6097) [hep-ph]
85. CMS Collaboration [CMS Collaboration], CMS-PAS-BTV-15-001
86. M. Cacciari, G.P. Salam, Phys. Lett. B **659**, 119 (2008). doi:[10.1016/j.physletb.2007.09.077](https://doi.org/10.1016/j.physletb.2007.09.077). [arXiv:0707.1378](https://arxiv.org/abs/0707.1378) [hep-ph]
87. M. Czakon, P. Fiedler, A. Mitov, Phys. Rev. Lett. **110**, 252004 (2013). doi:[10.1103/PhysRevLett.110.252004](https://doi.org/10.1103/PhysRevLett.110.252004). [arXiv:1303.6254](https://arxiv.org/abs/1303.6254) [hep-ph]
88. A. Bredenstein, A. Denner, S. Dittmaier, S. Pozzorini, JHEP **1003**, 021 (2010). doi:[10.1007/JHEP03\(2010\)021](https://doi.org/10.1007/JHEP03(2010)021). [arXiv:1001.4006](https://arxiv.org/abs/1001.4006) [hep-ph]
89. A. Bredenstein, A. Denner, S. Dittmaier, S. Pozzorini, Phys. Rev. Lett. **103**, 012002 (2009)
90. F. Febres Cordero, L. Reina, D. Wackerroth, Phys. Rev. D **80**, 034015 (2009). doi:[10.1103/PhysRevD.80.034015](https://doi.org/10.1103/PhysRevD.80.034015). [arXiv:0906.1923](https://arxiv.org/abs/0906.1923) [hep-ph]
91. G. Bevilacqua, M. Worek, JHEP **1207**, 111 (2012). doi:[10.1007/JHEP07\(2012\)111](https://doi.org/10.1007/JHEP07(2012)111). [arXiv:1206.3064](https://arxiv.org/abs/1206.3064) [hep-ph]
92. <https://twiki.cern.ch/twiki/bin/view/LHCPhysics/SingleTopRefXsec>. Accessed 10 Jan 2017
93. M. Aliev, H. Lacker, U. Langenfeld, S. Moch, P. Uwer, M. Wierdermann, HATHOR: hadronic top and heavy quarks cross section calculator. Comput. Phys. Commun. **182**, 1034 (2011). doi:[10.1016/j.cpc.2010.12.040](https://doi.org/10.1016/j.cpc.2010.12.040). [arXiv:1007.1327](https://arxiv.org/abs/1007.1327) [hep-ph]
94. P. Kant, O.M. Kind, T. Kintscher, T. Lohse, T. Martini, S. Mölbitz, P. Rieck, P. Uwer, HatHor, for single top-quark production: updated predictions and uncertainty estimates for single top-quark production in hadronic collisions. Comput. Phys. Commun.

- 191, 74 (2015). doi:[10.1016/j.cpc.2015.02.001](https://doi.org/10.1016/j.cpc.2015.02.001). arXiv:[1406.4403](https://arxiv.org/abs/1406.4403) [hep-ph]
95. I. Hinchliffe, F.E. Paige, M.D. Shapiro, J. Soderqvist, W. Yao, Phys. Rev. D **55**, 5520 (1997)
96. H. Bachacou, I. Hinchliffe, F.E. Paige, Phys. Rev. D **62**, 015009 (2000)
97. H. Baer, V. Barger, A. Lessa, X. Tata, Phys. Rev. D **86**, 117701 (2012)
98. U. Chattopadhyay, A. Datta, A. Datta, A. Datta, D.P. Roy, Phys. Rev. B **493**, 127 (2000)
99. J.K. Mizukoshi, P. Mercadante, X. Tata, Phys. Rev. D **72**, 035009 (2005)
100. R. Kadala, J.K. Mizukoshi, P. Mercadante, X. Tata, Eur. Phys. J. C **56**, 511 (2008)
101. <https://twiki.cern.ch/twiki/bin/view/LHCPhysics/SUSYCrossSections13TeVgluglu>
102. C. Borschensky, M. Krmer, A. Kulesza, M. Mangano, S. Padhi, T. Plehn, X. Portell, Eur. Phys. J. C **74**(12), 3174 (2014). doi:[10.1140/epjc/s10052-014-3174-y](https://doi.org/10.1140/epjc/s10052-014-3174-y). arXiv:[1407.5066](https://arxiv.org/abs/1407.5066) [hep-ph]
103. Y. Gershtein et al., arXiv:[1311.0299](https://arxiv.org/abs/1311.0299) [hep-ex]
104. A. Fowlie, arXiv:[1510.07319](https://arxiv.org/abs/1510.07319) [hep-ph]